Signal Processing 165 (2019) 104–114

Contents lists available at ScienceDirect

Signal Processing

journal homepage: www.elsevier.com/locate/sigpro

Retinal vessel segmentation by a divide-and-conquer funnel-structured classification framework

Xiaohong Wang, Xudong Jiang*

School of Electrical and Electronic Engineering, Nanyang Technological University, 639798, Singapore

ARTICLE INFO

Article history:
Received 27 December 2018
Revised 17 May 2019
Accepted 11 June 2019
Available online 12 June 2019

Keywords:
Retinal vessel segmentation
Divide-and-conquer
Multiplex vessel partition
Funnel-structured classification framework

ABSTRACT

Accurate vessel segmentation is a fundamental and challenging task for the retinal fundus image analysis. Current approaches typically train a global discriminative model for retinal vessel classification that is difficult to fit the complex pattern of vessel structure. In this paper, we propose a novel divide-and-conquer funnel-structured classification framework for retinal vessel segmentation. More specifically, a dividing algorithm, named multiplex vessel partition (MVP), is proposed to divide retinal vessel into well constrained subsets where vessel pixels with similar geometrical property are grouped. A set of homogeneous classifiers are trained in parallel to form discriminative decision for each group. This decomposes a complex classification problem into a number of relatively simpler ones. Moreover, a funnel-structured vessel segmentation (FsVS) framework is proposed to reclassify the uncertain samples caused by imperfect grouping of pixels. This alleviates the problem in data partition at the dividing phase and further enhances the complexity and discriminative capability of the decision model. Both quantitative and qualitative experimental comparisons on three publicly available databases show that the proposed framework produces high performance for retinal vessel segmentation, achieving 95.47–96.46% vessel segmentation accuracy, 83.72–85.79% local vessel segmentation accuracy, 78.63–81.92% F1-score and 76.55–80.13% Matthew correlation coefficient respectively, better than the state-of-the-art methods.

1. Introduction

Retinal vessel segmentation is an important part of computer-aided diagnosis of retinal diseases, like arteriosclerosis, vein occlusions, and diabetic retinopathy [1–3]. A reliable assessment for those diseases can be achieved by regularly performing accurate measurement of the vessel width, tortuosity and proliferation [4,5]. If abnormal signs are detected at early stage, timely treatment can be advised to perform on patients. Manual segmentation of retinal vessel is a tedious task that requires experience experts to annotate a huge amount of retinal images by hand, thus not feasible for large-scale research study and clinical utility. Vessel segmentation based on computer vision and image processing provides an efficient and economic benefit tool for retinal image analysis.

Many algorithms for automatic retinal vessel segmentation have been reported that can be generally divided into two groups: unsupervised and supervised methods. Unsupervised methods mainly focus on the inherent characteristic of the retinal vessel without the need of prior information from the manual annotated training data. Vessel tracking [6,7], morphological morphology [8,9], active contour [10–12] and graph-based approaches [13,14], are four popular unsupervised categories for retinal vessel segmentation. Supervised methods on the basis of pixel classification rules assign each pixel to be vessel or non-vessel. *K*-nearest neighbors algorithm (KNN) [15], Gaussian mixture model (GMM) [16], support vector machine (SVM) [17,18], neural network (NN) [19,20], random forest classifier(RFC) [21,22], are five widely used decision models in retinal vessel segmentation system. Fraz et al. [23] utilized an ensemble classifier of boosted and bagged decision trees to distinguish vessel from background. Gu et al. [24] extracted the context distance features together with the structured features for vessel classification based on the boosted tree classifier. Classification results produced by fuzzy logic, artificial NN and SVM, were fused together by Barkana et al. [25]. In [26], a cascade classification network that enveloped a set of computationally efficient Mahalanobis distance classifiers was proposed to form a highly nonlinear decision boundary for retinal vessel classification.

Deep learning based methods demonstrate superior performance in image recognition, such as semantic segmentation [27,28], and image classification [29]. Recently, they have also been successfully applied to retinal vessel segmentation [30–40]. Yan et al. [35] jointly adopted both the segment-level and the

* Corresponding author.
E-mail addresses: E150023@e.ntu.edu.sg (X. Wang), exdjiang@ntu.edu.sg (X. Jiang).

https://doi.org/10.1016/j.sigpro.2019.06.018
0165-1684/

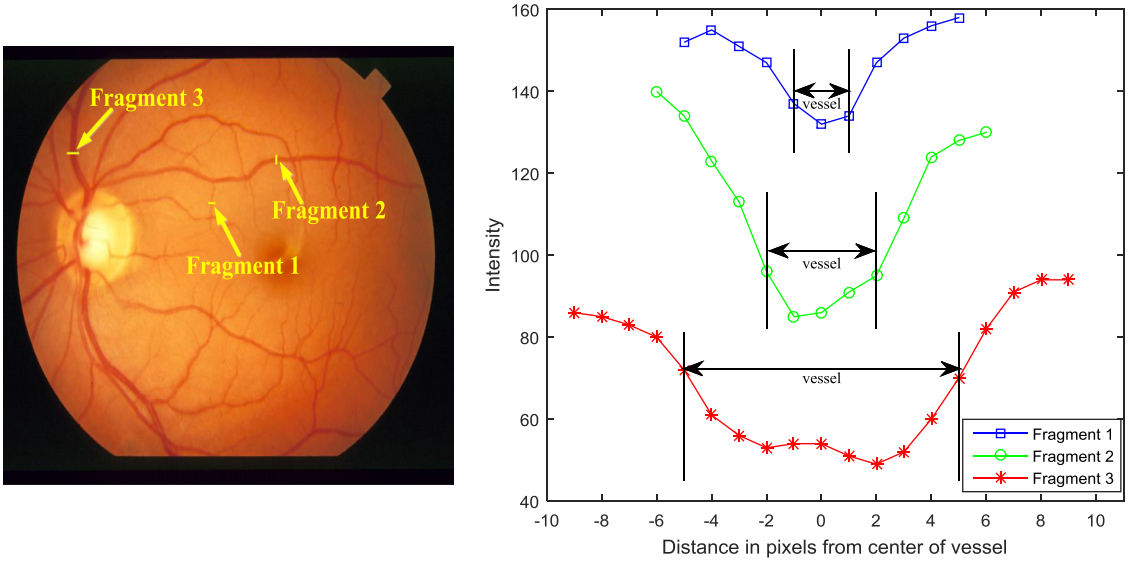

Fig. 1. Intensity profile of cross section of three representative vessel fragments. The first column: fundus image with three vessel fragments (vessel width: Fragment 1 < Fragment 2 < Fragment 3). The second column: intensity profile of cross section of fragments marked in fundus image.

pixel-level losses to train the deep learning network. Oliveira et al. [36] combined the stationary wavelet transform with a multiscale fully convolutional neural network for vessel structure delineation. Hu et al. [37] applied a multiscale convolutional neural network with an improved cross-entropy loss for retinal vessel detection. Yan et al. [38] divided the vessel segmentation task into three subtasks, each of which was trained by a deep learning model using a unique pixel-wise loss. Yu et al. [39] used the segmentation result generated by deep neural network to hierarchically divide retinal vessel tree. Feng et al. [40] proposed a cross-connected convolutional neural network (CcNet) for the automatic retinal vessel segmentation.

Supervised methods usually perform better than the unsupervised ones on retinal vessel segmentation. Nevertheless, the decision boundary between vessel and non-vessel is sometimes hard to be determined. Fig. 1 shows intensity profile of cross section of three representative vessel samples. Intensity profile varies with the vessel scale, e.g. vessels with large scale tend to be darker than those with small scale. In addition, since vessels almost never have ideal step edges [41], intensity of vessels near the center differ from those located at edge. Previous methods treat all vessel pixels equally and train a global discriminative model for retinal vessel detection. The large geometrical structure difference among retinal vessels with different scale and position greatly limits the precision of the decision boundary of the global discriminative model.

Motivated by that it is extremely difficult to handle the large variation of vessel pixels by learning a single global discriminative model, we develop a novel divide-and-conquer funnel-structured classification framework for retinal vessel segmentation. Main contributions of our work include: first, we propose a multiplex vessel partition method to divide the retinal vessel pixels into well constrained subsets where vessel pixels with similar geometrical property are assigned together. This multiplex vessel partition method decomposes the complex vessel pixel pattern into a number of homogeneous patterns, making each of them easier to be classified from the non-vessel pixels. Thus, a set of homogeneous classifiers are trained in parallel to form discriminative model for each subset. Training a retinal vessel model in each subset leads to two benefits: one is that it reduces the computation cost like time and storage and the other is that it makes the vessel pixels more separable from the non-vessel pixels as vessel samples in the same subset have smaller variation. Second, we propose a funnel-structured vessel segmentation framework to reclassify the uncertain samples caused by imperfect data partition in the dividing phase. This further enhances the complexity and discriminative capability of the decision model. Our approach achieves high performance for retinal vessel segmentation consistently on all three diverse databases, better than the state-of-the-art methods. To the best of our knowledge, this is the first published work for retinal vessel segmentation under a funnel-structured segmentation framework with the divide-and-conquer strategy. In addition, the proposed framework can also be extended to other general image segmentation tasks.

2. Proposed method

In this section, we describe the details of our proposed hierarchical architecture for retinal vessel segmentation based on divide-and-conquer strategy. The proposed divide-and-conquer funnel-structured architecture is shown in Fig. 2. First, we propose a multiplex vessel partition (MVP) method to divide retinal image pixels into 6 subsets on the basis of their geometric property, i.e. three scales (small, medium, and large) and two positions (edge and center) for each scale. For each of the 6 subsets, a classifier is trained to classify the data into vessel pixels, non-vessel pixels and uncertain pixels. Second, we feed the classified uncertain samples from each subset to the proposed funnel-structured vessel segmentation (FsVS) framework, which concatenates the classification decision at three levels. The 1st level of FsVS utilizes the information of 6 subsets separately; the 2nd level of FsVS merges the uncertain samples of six subsets to three subsets, i.e. combine the pixels with the same scale but different position into one subset; the 3rd level of FsVS groups all uncertain samples to be a global subset. With this funnel-structured architecture, we reduce the classification error caused by the imperfect partition at the dividing phase and enhance the complexity and discriminative capability of the decision model.

2.1. Multiplex vessel partition

To divide retinal vessel into a compact subset, we propose a multiplex vessel partition method based on Gabor wavelet transformation. Gabor filter has been widely applied to retinal image

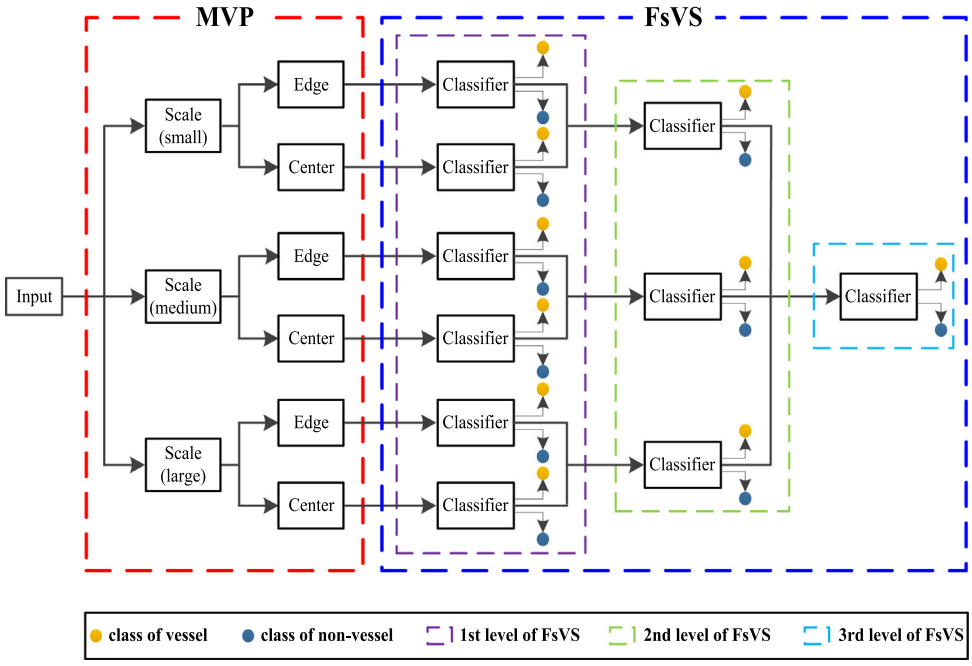

Fig. 2. The proposed divide-and-conquer funnel-structured architecture for retinal vessel segmentation.

analysis [10,16,23,42] thanks to its biological relevance and superior mathematic property. A 2-D Gabor wavelet kernel is the product of an elliptical Gaussian envelope and a complex plane wave, expressed as [23]

$$\varphi_{\lambda,\sigma,\gamma,\theta}(x,y) = \exp\left(-\frac{x'^2+\gamma y'^2}{2\sigma^2}\right)\exp\left(i2\pi\frac{x'}{\lambda}\right), \quad (1)$$

where $x' = x\cos\theta + y\sin\theta$ and $y' = -x\sin\theta + y\cos\theta$. θ denotes the orientation of Gabor wavelet. λ is the wavelength of the sinusoidal factor. σ and γ symbolize the scale of the Gaussian envelope and the ellipticity of the Gabor filter respectively.

For a given pixel at (x, y) in an image $I \in \mathbb{R}^2$ ($\mathbb{R}^2$ denotes the real plane), the Gabor wavelet transformation of $I(x, y)$ is obtained by convolving $I(x, y)$ with Gabor kernel $\varphi_{\lambda,\sigma,\gamma,\theta}$, given by

$$J_{\lambda,\sigma,\gamma,\theta}(x,y) = I(x,y) * \varphi_{\lambda,\sigma,\gamma,\theta}(x,y). \quad (2)$$

The magnitude of $J_{\lambda,\sigma,\gamma,\theta}(x, y)$ is computed as

$$A_{\lambda,\sigma,\gamma,\theta}(x,y) = \sqrt{\mathrm{Re}(J_{\lambda,\sigma,\gamma,\theta}(x,y))^2 + \mathrm{Im}(J_{\lambda,\sigma,\gamma,\theta}(x,y))^2}, \quad (3)$$

where $\mathrm{Re}(J_{\lambda,\sigma,\gamma,\theta}(x, y))$ and $\mathrm{Im}(J_{\lambda,\sigma,\gamma,\theta}(x, y))$ represent the real and imaginary parts of $J_{\lambda,\sigma,\gamma,\theta}(x, y)$ respectively. Generally, the real part of a Gabor wavelet kernel is used as a smooth filter while its imaginary part is regarded as edge detector. As the Gabor wavelet transformation is applied in a finite local window centered at (x, y), we normalize both the real and the imaginary parts of Gabor filter coefficients to be zero mean and the unit sum of the absolute values, respectively.

Our proposed multiplex vessel partition (MVP) method partitions vessel into different subsets based on two crucial properties of Gabor wavelet transformation. First, Gabor filter can be tuned to capture the vessel width, since the Gabor wavelet transformation with the scale that best matches for vessel yields the maximum magnitude value $A_{\lambda,\sigma,\gamma,\theta}(x, y)$. Second, Gabor wavelet transformation produces higher absolute value of its real part than its imaginary part, i.e. $|\mathrm{Re}(J_{\lambda,\sigma,\gamma,\theta}(x, y))| > |\mathrm{Im}(J_{\lambda,\sigma,\gamma,\theta}(x, y))|$ for pixels located near the vessel center. Similarly, for pixels near the vessel edge we have $|\mathrm{Im}(J_{\lambda,\sigma,\gamma,\theta}(x, y))| > |\mathrm{Re}(J_{\lambda,\sigma,\gamma,\theta}(x, y))|$.

Algorithm 1 shows the details of our proposed multiplex vessel partition. For each vessel pixel $I(x, y)$, we are interested in the maximum magnitude of the Gabor wavelet transformation over different orientations at a given scale. In this paper, a Gabor wavelet kernel is rotated within twelve orientations at step of $\pi/12$, i.e. $\theta = [0, \pi/12, \ldots, 11\pi/12]$. The maximum magnitude of the Gabor wavelet transform over all orientations for each scale σ_h is marked as $A'_{\lambda,\sigma_h,\gamma,\theta_p}(x, y)$. By capturing the maximum value of $A'_{\lambda,\sigma_h,\gamma,\theta_p}(x, y)$ over all scales $\sigma_h, h \in 1, 2, \ldots, m$, we assign the pixel $I(x, y)$ into the subset with the scale that best matches the vessel width. In this paper, scale $\sigma_h (h \in 1, 2, \ldots, m)$ is selected from the set of [2,4,6] that span the possible widths of vessels throughout the retinal images. Parameters γ, and λ are set to be the same as those used in [10] for a good delineation of the vessel geometrical structure. To check a retinal vessel $I(x, y)$ near to the vessel center or edge, we propose a position decision rule: if the absolute value of the real part of the Gabor wavelet transformation $|\mathrm{Re}(J_{\lambda,\sigma,\gamma,\theta}(x, y))|$ is larger than that of its imaginary part $|\mathrm{Im}(J_{\lambda,\sigma,\gamma,\theta}(x, y))|$, the pixel $I(x, y)$ is assigned to a center cluster; otherwise it is assigned to an edge cluster.

To make our proposed method produce balanced number of pixels between vessel center cluster and edge cluster for noisy and low contrast retinal image, a weight τ is introduced to control the partitioned proportion of center and edge clusters. Fig. 3 shows the partition results based on different τ. Clearly, a smaller value of τ leads to more pixels assigned to edge cluster. From this observation, we set τ to be 0.5 to have a balanced partition. Moreover, Fig. 3 visibly exemplifies that the proposed method can effectively divide vessel pixels into clusters based on their geometrical property. Even for the small scale retinal vessel (fragment in the first row of Fig. 3), the proposed method also performs well to divide pixels into the center and edge clusters.

The proposed multiplex vessel partition (MVP) method is targeted at dividing the complex vessel patterns of large variation into a number of homogeneous groups of patterns. Non-vessel pixels are also portioned according the same rules. It is an unsupervised dividing strategy that is conducted on training and test samples independently, without learning from data. By dividing the samples with different geometrical property into a compact subset efficiently and robustly, we decompose the complex vessel pattern

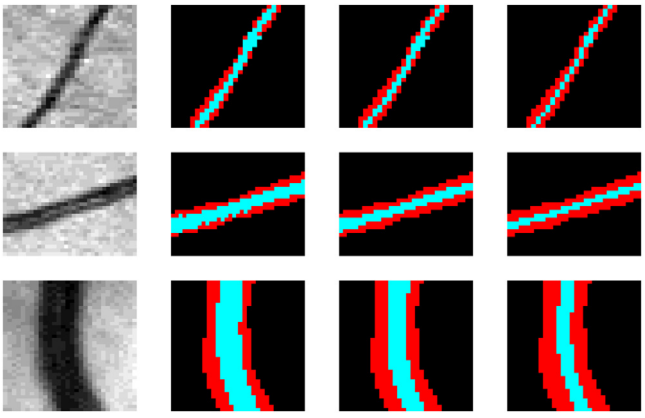

Fig. 3. Examples of vessel pixels dividing results based on different τ. The top to the bottom row of the first column: fundus image fragments with scales from small to large. The second to the last column: vessel pixels dividing results at τ=1, 0.75, 0.5, respectively. Red color marks pixels assigned to the edge cluster and blue color marks pixels assigned to the center cluster. (For interpretation of the references to colour in this figure legend, the reader is referred to the web version of this article.)

into a number of homogeneous patterns. This greatly reduces the variation of the vessel pattern in each group. Therefore, the difficult vessel segmentation problem can be conquered by decomposing it into a number of easier sub-problems and solve (conquer) them one by one.

2.2. Funnel-structured vessel segmentation

Based on the proposed MVP scheme, the entire training sample is grouped into a number of subsets C_{qg} and C_{qe} (Algorithm 1).

Algorithm 1 Multiplex Vessel Partition.

Require: Sample $I(x, y)$, Gabor wavelet kernel $\varphi_{\lambda,\sigma,\gamma,\theta}$;
Ensure: Subsets C_{qg} and C_{qe};
1: **for** h = 1 to m **do**
2: **for** w = 1 to n **do**
3: $J_{\lambda,\sigma_h,\gamma,\theta_w}(x, y) = I(x, y) * \varphi_{\lambda,\sigma_h,\gamma,\theta_w}(x, y)$;
4: **end for**
5: Decide: $\theta_p = \underset{\theta_{w,w\in 1,2,\ldots,n}}{\operatorname{argmax}} A_{\lambda,\sigma_h,\gamma,\theta_w}$;
6: $A'_{\lambda,\sigma_h,\gamma,\theta_p}(x, y) = |J_{\lambda,\sigma_h,\gamma,\theta_p}(x, y)|$;
7: **end for**
8: Decide: $\sigma_q = \underset{\sigma_{h,h\in 1,2,\ldots,m}}{\operatorname{argmax}} A'_{\lambda,\sigma_h,\gamma,\theta_p}(x, y)$;
9: **if** $\tau \times |\mathrm{Re}(J_{\lambda,\sigma_q,\gamma,\theta_p}(x, y))| > |\mathrm{Im}(J_{\lambda,\sigma_q,\gamma,\theta_p}(x, y))|$ **then**
10: $I(x, y)$ is assigned to cluster Cqg, g indicates a center cluster;
11: **else**
12: $I(x, y)$ is assigned to cluster Cqe, e indicates an edge cluster;
13: **end if**

Let C_k index the subsets C_{qg} and C_{qe}. Our next step is to conquer each subset C_k separately by training a discriminative model locally. With each subset C_k, we train a non-linear SVM classifier because of its well-known good generalization and popular application in binary vessel classification problem [17,25,43]. To circumvent the unavoidable partition error by the MVP scheme, we propose a funnel-structured vessel segmentation (FsVS) framework. It classifies the data in each subset C_k into three classes (vessel pixels, non-vessel pixels and uncertain pixels) and concatenates the uncertain pixels for further classification. The first level of FsVS utilizes information of each subset separately. The second level of

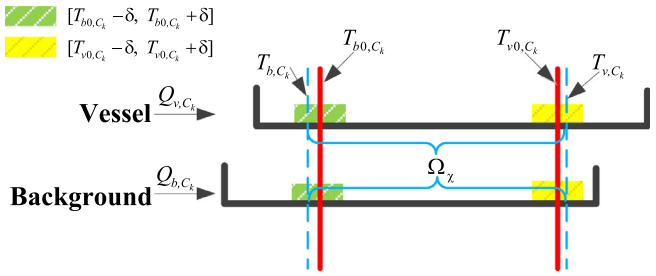

Fig. 4. Threshold searching process. Shaded areas in green and yellow color are the searching range $[T_{v0,C_k}-\delta,\ T_{v0,C_k}+\delta]$ and $[T_{b0,C_k}-\delta,\ T_{b0,C_k}+\delta]$ respectively. Pixels in the region Ω_χ remain to be further processed at the subsequent level. (For interpretation of the references to colour in this figure legend, the reader is referred to the web version of this article.)

FsVS merges the uncertain samples of six subsets to three subsets for further classification by combining the vessel with the same scale but different position into the one subset. The last level of FsVS groups all uncertain samples to be a global subset to finally classify it into two classes. With this funnel-structured architecture, we reduce the classification error caused by the imperfect partition at the dividing phase and enhance the complexity and discriminative capability of the whole decision model.

Let $S_{\mathbf{x}_j,C_k}$, $j \in [1, 2, \ldots, N_{C_k}]$, represent the training sample in subset C_k, where $\mathbf{x}_j$ is the feature vector of the training sample. Assigning $S_{\mathbf{x}_j,C_k}$ to be vessel Ω_v, background Ω_b or uncertain class Ω_χ, is decided by

$$S_{\mathbf{x}_j,C_k} \in \begin{cases} \Omega_v, & if\ P(S_{\mathbf{x}_j,C_k}) > T_{v,C_k}, \\ \Omega_b, & if\ P(S_{\mathbf{x}_j,C_k}) < T_{b,C_k}, \\ \Omega_\chi, & if\ T_{b,C_k} \le P(S_{\mathbf{x}_j,C_k}) \le T_{v,C_k}, \end{cases} \tag{4}$$

where $P(S_{\mathbf{x}_j,C_k})$ is the output of SVM classification that denotes the probability of the pixel belonging to the vessel. Thresholds T_{v,C_k} and T_{b,C_k} control the decision of $S_{\mathbf{x}_j,C_k}$ belonging to the vessel or background. Samples falling in the class Ω_χ remain to be further processed at the higher level of funnel-structured vessel segmentation framework. In this paper, we design a threshold searching method to select appropriate thresholds T_{v,C_k} and T_{b,C_k}. First, the probability distribution of vessel and background of training data in the subset C_k are sorted as ascending order respectively, resulting in two sequences Q_{v,C_k} and Q_{b,C_k}. Then, we define two initial thresholds T_{v0,C_k} and $T_{b0,Ck}$ whose values yield about 60% and 30% training samples removal (being classified into either vessel Ω_v or background Ω_b) in the first two levels of FsVS, with remaining 10% training pixels for training decision model in the last level of FsVS.

To fine-tune both T_{v0,C_k} and T_{b0,C_k}, a searching scheme is formulated as:

$$\text{Decide}: T_{v,C_k} = \underset{T'_v}{\operatorname{argmin}} \frac{\Gamma[Q_{v,C_k} > T'_v]}{\Gamma[Q_{v,C_k} > T'_v] + \Gamma[Q_{b,C_k} > T'_v]}, \tag{5}$$

and

$$\text{Decide}: T_{b,C_k} = \underset{T'_b}{\operatorname{argmin}} \frac{\Gamma[Q_{b,C_k} < T'_b]}{\Gamma[Q_{v,C_k} < T'_b] + \Gamma[Q_{b,C_k} < T'_b]}, \tag{6}$$

where $T'_v \in [T_{v0,C_k}-\delta,\ T_{v0,C_k}+\delta]$ and $T'_b \in [T_{b0,C_k}-\delta,\ T_{b0,C_k}+\delta]$. $\Gamma[\cdot]$ is the function of counting the length of sequence. δ is the searching range around T_{v0,C_k} and T_{b0,C_k}. Fig. 4 shows the proposed process of the threshold searching. According to the searching rule of (Eqs. (5)-(6)), we achieve the smallest classification error for vessel and background within the range of 2δ centered at T_{v0,C_k} and T_{b0,C_k} respectively. Parameter δ is limited to a small value that makes threshold searching among 200 samples around T_{v0,C_k} and T_{b0,C_k} compared to approximately $0.1 \sim 1$ million vessel and background training samples. The threshold at the last level of the FsVS

is set to be the one that produces the maximum accuracy on the training set. Our proposed funnel-structured vessel segmentation framework greatly reduces the classification error caused by the imperfect partitions at the dividing phase. Moreover, the proposed hierarchal classification structure enhances the complexity and discriminative capability of the decision model comparing to a single SVM model.

In test procedure, a testing sample is assigned into one of the six subsets based on the proposed multiplex vessel partition scheme in the same way as the training samples. It will be classified into either vessel pixel or background pixel by Eq. (4) in one and only one of the 20 outputs of the proposed funnel-structured architecture as shown in Fig. 2.

2.3. Feature representation of image pixel

To alleviate the effect of intensity fluctuation and random noise during image acquisition, a preprocessing method proposed in our previous published work [42] is applied to enhance retinal image quality. It normalizes the background based on the median filter and removes impulsive noise while preserving the vessel details by the image detail preserving truncation filter [44]. We evaluate our proposed method with features that have been widely used in the literature of retinal image analysis, including Gabor wavelt transformation (total 8 features) [23], matched filter (total 32 features) [41], gray-level-based feature (total 35 features) [19], Frangi filter (total 20 features) [45] and Difference of Gaussian (total 5 features) [46]. All features are normalized independently to be zero mean and unit variance over the field of view (FOV) of its image. Features from all red, green and blue channels, are weighted and concatenated together. To remove the unreliable dimensions of feature vector and construct a more compact and discriminative feature space, a dimensionality reduction method named asymmetric principal component analysis (APCA) [47] is applied to reduce the feature dimensionality to be its one-third, i.e. the same feature dimensionality as a single color channel.

2.4. Post-processing

From visual inspection of the vessel segmentation result, the loss of segmented retinal vessels (like thin vessels) and the false detection of pathological regions, often appear in retinal vessel classification results, which causes the reduction of vessel segmentation accuracy [19,20,22]. To enhance the segmentation performance for retinal vessel, we apply a post-processing method proposed in our previous published work [48]. This post-processing method firstly connects the discontinuous thin vessel fragments on the basis of mathematical morphological operations. Then, the pathological regions that are difficult to be distinguished from retinal vessels are automatically removed by the comparison of the geometric structure of vessels and pathological regions.

3. Experimental evaluation

3.1. Materials

To evaluate the performance of our proposed vessel segmentation framework, extensive experiments are performed on four standard publicly available databases:

- The DRIVE database [15] contains 40 color fundus images (565 × 584 pixels) captured by Canon CR5 nonmydriatic 3 charge-coupled-device cameras at 45° field of view. This database is divided into two sets: training set and test set, and both comprise 20 fundus images. Two manual segmentations for each image in test set are provided, and the first manual segmentation result is taken as the ground truth.
- The STARE database [49] includes 20 color fundus images (700 × 605 pixels) captured by a TopCon TRV-50 fundus camera at 35° field of view. Ten images of STARE databases are healthy while the other half images contain abnormalities. Two observers manually segment all the retinal images in the STARE database, and the result of the former one is considered as ground truth.
- The CHASE_DB1 database [23] consists of 28 color fundus images (999 × 960 pixels) captured by a hand-held Nidek NM-200-D fundus camera at 30° field of view. CHASE_DB1 database is a part of the Child Heart and Health study in England. Two manual segmentations for this database are provided while the first of them is deployed as the ground truth.
- The HRF database [50] comprises 15 images from diabetic retinopathy patients, 15 images from glaucomatous patients, and 15 images from healthy patients. Images (3504 × 2336 pixels) are captured by a Canon CF-60 UVi equipped with Canon EOS 20D digital camera at 60° field of view. One manual segmentation for each retinal image is taken as ground truth.

The training and testing set are separated by DRIVE database. For STARE database, the leave-one-out strategy is performed [15,16,18,22,30,31], i.e. each image is tested using a discriminative model trained by the other 19 images. For the CHASE_DB1 database, the first 20 images are utilized for training while the remaining 8 images are applied for testing [30]. For the HRF database, we take the first 5 images of each subset for training while all the remaining images for testing [18,35]. To reduce the computational cost of experimental evaluation, images and labels on HRF database are down-sampled by a factor of 4, and the segmentation results are then up-sampled to the original size for quality evaluation [35]. In addition, we only consider the pixels in the field of view (FOV) in each retinal image. For DRIVE and HRF, the original FOVs are provided by the database. For STARE and CHASE_DB1, FOVs are not provided and we compute them using the program as [16,23,30,43].

3.2. Evaluation criterion

Performance of the proposed method is quantitatively analyzed by comparing the segmented result with the ground truth provided by each database. Four different measurements for vessel segmentation performance evaluation are employed in this paper, including the segmentation accuracy (ACC), local segmentation accuracy (ACC_l), F1-score (F1) and Matthews correlation coefficient (MCC). ACC is the ratio of the number of correctly classified pixels to the total number of pixels within the field of view (FOV). Since background pixels that are easily detected occupy more than 80% pixels of FOV, different methods only have a small discrimination in terms of the global accuracy ACC [4]. ACC_l evaluates the segmentation accuracy of the local area which consists of vessel and its neighbourhood within a certain distance from the center of vessel [4]. We generate this local area by the morphological dilation operation with a disc structuring element. The radius of structuring element is set to be the value that forms the local area where the number of vessel and background pixels are balanced. F1 and MCC, two widely used measurements in recent vessel segmentation works [18,20,22,24,51], are effective to assess performance on the unbalanced database. They are given by

$$\mathrm{F1} = \frac{2(\mathrm{TP}/(\mathrm{TP}+\mathrm{FP})) \times (\mathrm{TP}/(\mathrm{TP}+\mathrm{FN})))}{\mathrm{TP}/(\mathrm{TP}+\mathrm{FP}) + \mathrm{TP}/(\mathrm{TP}+\mathrm{FN})}, \tag{7}$$

and

$$\mathrm{MCC} = \frac{\mathrm{TP} \times \mathrm{TN} - \mathrm{FP} \times \mathrm{FN}}{\sqrt{(\mathrm{TP}+\mathrm{FP})(\mathrm{TP}+\mathrm{FN})(\mathrm{TN}+\mathrm{FP})(\mathrm{TN}+\mathrm{FN})}}, \tag{8}$$

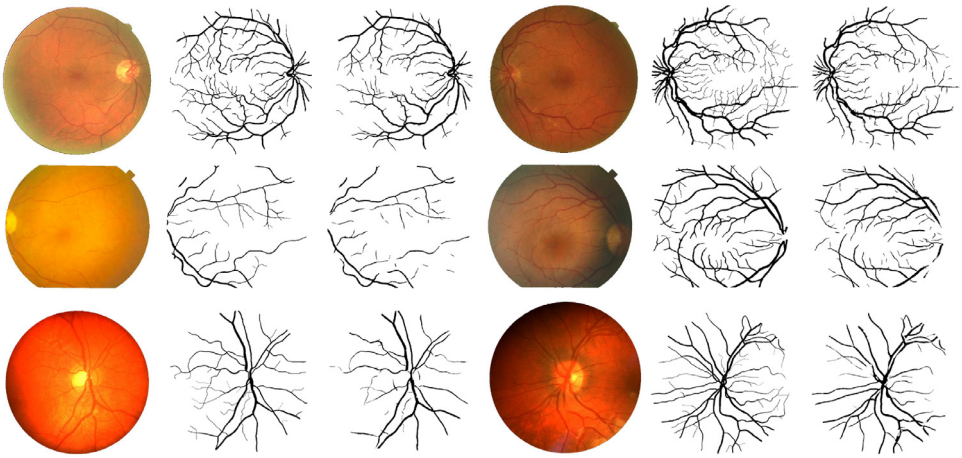

Fig. 5. Examples of segmentation results. The first row to the third row: images and their segmentation results on DRIVE, STARE and CHASE_DB1 databases. The first column to the last column: for the best segmentation case, original image, ground truth, segmentation result; for the worst segmentation case, original image, ground truth, segmentation result.

Table 1
Segmentation performance on DRIVE, STARE and CHASE_DB1 databases(%).

Database	Method	ACC	ACC_l	F1	MCC
DRIVE	2nd human observer	94.73	82.10	78.91	75.91
	Singel SVM	95.16	82.41	78.78	76.77
	Proposed method	**95.47**	**83.72**	**81.44**	**78.95**
STARE	2nd human observer	93.49	81.10	74.18	72.08
	Singel SVM	96.10	84.67	79.51	77.74
	Proposed method	**96.46**	**85.79**	**81.92**	**80.13**
CHASE_DB1	2nd human observer	96.13	81.58	79.73	77.67
	Singel SVM	95.69	78.66	75.46	73.19
	Proposed method	**96.17**	**80.70**	**78.63**	**76.55**

where TP and TN denote the number of pixels correctly classified as vessel and background, respectively; FN and FP represent the number of pixels incorrectly classified as the background and vessel, respectively.

3.3. Comparison to the single SVM classifier

Segmentation performance of the proposed framework and a single SVM classifier with the same pre-processing, feature representation and post-processing on the three public databases are shown in Table 1. In addition, the segmentation performance of the second human observer is also computed in Table 1 for reference. It shows that the segmentation performance of the proposed method are better than the single SVM classifier consistently over the 4 different evaluation criteria and consistently over the 3 different data sets. The comparison of the proposed framework to the single SVM classifier shown in Table 1 demonstrates the consistent performance gain brought by the proposed framework in this paper as they use the same methods of pre-processing, feature representation, classifier and post-processing. Note that other techniques of the pre-processing, feature representation, classifier and post-processing can also be applied in our proposed framework.

Fig. 5 shows the best and worst segmentation cases in DRIVE, STARE and CHASE_DB1 databases respectively. The ACC, ACC_l, F1 and MCC of the best case for DRIVE database are 96.70%, 87.69%, 86.54%, and 84.68%, while those measures of the worst case are 94.45%, 81.74%, 79.54% and 76.62%, respectively. For the STARE database, the values of the best case are 97.65%, 83.75%, 79.41% and 78.22%, and the values of the worst case are 94.26%, 79.74%, 76.14% and 74.26%, respectively. For the CHASE_DB1 database, the best case measures are 97.03%, 82.73%, 80.52% and 78.92%, and the worst case measures are 95.30%, 79.30%, 77.50% and 74.88%, respectively. Fig. 5 visualizes that the proposed method produces a high matching confidence between the segmentation result and the ground truth, integrating complex structures to the vessel tree with small false negative error.

3.4. Comparison to other published methods

3.4.1. Quantitative analysis

Table 2 shows the performance of different vessel segmentation methods in terms of ACC and ACC_l on DRIVE, STARE and CHASE_DB1 databases. CHASE_DB1 database was built in 2012, thus no result before this year is available. All methods used for comparison report their segmentation accuracy ACC. We compute the local accuracy ACC_l of the published methods based on the segmented images provided by their respective publications, like [4,5,16,18,19,34,49,51]. Table 2 shows that the proposed framework achieves better segmentation performance than those state-of-the-art methods in terms of the both ACC and ACC_l consistently over all the 3 databases. Though the improvement of segmentation accuracy ACC between the proposed and other methods is marginal, the local segmentation accuracy ACC_l is visibly higher, about 2%-3% enhancement. High value of ACC_l is important for vessel segmentation algorithms because it indicates their discriminative ability of vessel from its boundary. High ACC_l produced by the proposed method exemplifies the effectiveness of it in retinal vessel segmentation. Recently, many powerful deep learning based approaches perform well on the separation of vessel and background from fundus images. Our proposed method produces better segmentation performance than most of the compared deep learning based approaches. Though our segmentation accuracy are slightly lower than Oliveira et al. [36] (i.e. ACC only 0.5% less than it on all 3 databases), we achieve more efficient vessel segmentation architecture without the need of training large number of parameters, extracting patches from each image and predicting the retinal map throughout every single patch. Comparison results between deep learning based methods and the proposed technique demonstrate the high potential of our designed none-deep learning model in dealing with vessel segmentation problem.

Fig. 6 shows the local accuracy of different methods with the different ratio of the number of pixels of background to that of vessel, obtained by increasing radius of structuring element from 1 to 15 on DRIVE, STARE and CHASE_DB1 databases respectively. Local accuracy at the small ratio of background to vessel indicates the

Table 2
Performance comparison with other methods in terms of ACC (%) and ACC_l (%).

Year	Method	DRIVE		STARE		CHASE_DB1	
		ACC	ACC_l	ACC	ACC_l	ACC	ACC_l
2016	Li et al. [30]*	95.27	N.A	96.28	N.A	95.81	N.A
2016	Fu et al. [32]*	94.70	N.A	95.45	N.A	N.A	N.A
2016	Fu et al. [34]*	95.23	81.44	95.85	82.62	94.89	75.70
2018	Yan et al. [35]*	95.42	N.A	96.12	N.A	96.10	N.A
2018	Oliveira et al. [36]*	**95.76**	N.A	**96.94**	N.A	**96.53**	N.A
2018	Hu et al. [37]*	95.33	N.A	96.32	N.A	N.A	N.A
2019	Yan et al. [38]*	95.38	N.A	96.38	N.A	96.07	N.A
2019	Yu et al. [39]*	95.24	N.A	96.13	N.A	N.A	N.A
2019	Feng et al. [40]*	95.28	N.A	96.33	N.A	N.A	N.A
2000	Hoover et al. [49]	N.A	N.A	92.67	77.54	N.A	N.A
2004	Staal et al. [15]	95.16	N.A	N.A	N.A	N.A	N.A
2006	Soares et al. [16]	94.66	80.97	94.80	81.58	N.A	N.A
2007	Perez et al. [1]	93.16	76.70	91.96	76.07	N.A	N.A
2011	You et al. [17]	94.34	N.A	94.97	N.A	N.A	N.A
2011	Marin et al. [19]	94.48	80.50	95.26	N.A	N.A	N.A
2012	Fraz et al. [23]	94.80	N.A	95.34	N.A	94.69	N.A
2013	Nguyen et al. [4]	94.07	81.73	93.24	81.37	N.A	N.A
2015	Roychowdhury et al. [5]	94.90	77.17	95.60	79.49	94.67	N.A
2015	Azzopardi et al. [51]	94.42	80.20	94.97	82.16	93.87	74.53
2017	Orlando et al. [18]	94.54	81.80	94.89	83.08	94.59	78.02
2017	Zhang et al. [22]	94.66	N.A	95.47	N.A	95.02	N.A
–	**Proposed method**	**95.47**	**83.72**	**96.46**	**85.79**	**96.17**	**80.70**

* Result produced by deep learning based method.

Table 3
Performance comparison with other methods in terms of F1-SCORE (%) and MCC (%).

Year	Method	DRIVE		STARE		CHASE_DB1	
		F1	MCC	F1	MCC	F1	MCC
2000	Hoover et al. [49]	N.A	N.A	65.42	61.34	N.A	N.A
2006	Soares et al. [16]	77.59	74.81	74.06	71.23	N.A	N.A
2011	Marin et al. [19]	76.16	73.53	N.A	N.A	N.A	N.A
2013	Nguyen et al. [4]	76.06	72.71	70.99	67.74	N.A	N.A
2015	Roychowdhury et al. [5]	72.85	69.45	72.97	70.36	N.A	N.A
2015	Azzopardi et al. [51]	77.64	74.75	76.18	73.35	70.90	68.02
2015	Vega et al. [20]	68.84	66.17	60.82	59.27	N.A	N.A
2016	Fu et al. [34]*	78.75	76.05	78.41	76.17	73.72	70.90
2017	Zhang et al. [22]	79.53	76.73	78.15	76.08	75.81	73.24
2017	Gu et al. [24]	78.86	75.89	79.53	77.24	72.02	69.28
2017	Orlando et al. [18]	78.57	75.56	76.44	74.17	73.32	70.46
–	**Proposed method**	**81.44**	**78.95**	**81.92**	**80.13**	**78.63**	**76.55**

* Result produced by deep learning based method.

ability of the segmentation method to distinguish pixels around vessel edges. The errors for local region are often resulted from the merging of parallel vessel, the missing of low contrast vessel, and the coarse delineation of vessel edge. With the increasing ratio of background to vessel, more background pixels far away from vessel are counted in the computation of the accuracy and the accuracy curve tends to be stable. Accuracy improvement of our segmentation method with respect to other segmentation methods at different ratio of background to vessel is clearly shown in Fig. 6. Consistently better performance yielded by the proposed segmentation framework demonstrates its capability to generate accurate decision boundary between vessel and background.

Table 3 shows the comparison of F1 and MCC between the proposed method and other state-of-the-art methods on DRIVE, STARE and CHASE_DB1 databases. Values of F1 and MCC for [4,5,16,19,34,49,51], are computed by the segmented images from their corresponding publications. Our method reports the statistically noticeable improvement of F1 and MCC consistently over the 3 databases, displaying advantage of the proposed framework for vessel classification where the samples in two classes (vessel and background) are unbalanced.

3.4.2. Qualitative analysis

The proposed method works well on vessel segmentation of fundus images, including some complex structures that are difficult to be correctly detected by many state-of-the-art methods. Four specific challenging and difficult conditions of retinal images are shown in the first row of Fig. 7, i.e. closely parallel vessels, low contrast vessels, crossing vessels, and lesions. In Fig. 7, we compare the segmentation results under those four conditions of our proposed method with methods by [4,5,16,18,34,51]. Better segmentation performance of the proposed vessel segmentation framework is visible in Fig. 7, e.g. distinguish closely parallel vessels, detect vessels with low contrast, and preserve the structure between crossing vessels and remove pathological regions. One reason is that we design a hierarchical architecture for retinal vessel segmentation, thus vessels at branch and boundary that differ from the majority of vessels are able to be correctly detected, avoiding the merging of closely parallel vessels, or the coarse delineation of branch and boundary vessels, which are challenging problems in many compared methods. Aforementioned representative examples shown in Fig. 7 also provide a visual evidence that our proposed method is capable of maintaining the integrity of vessel tree under challenging and difficult conditions of retinal image.

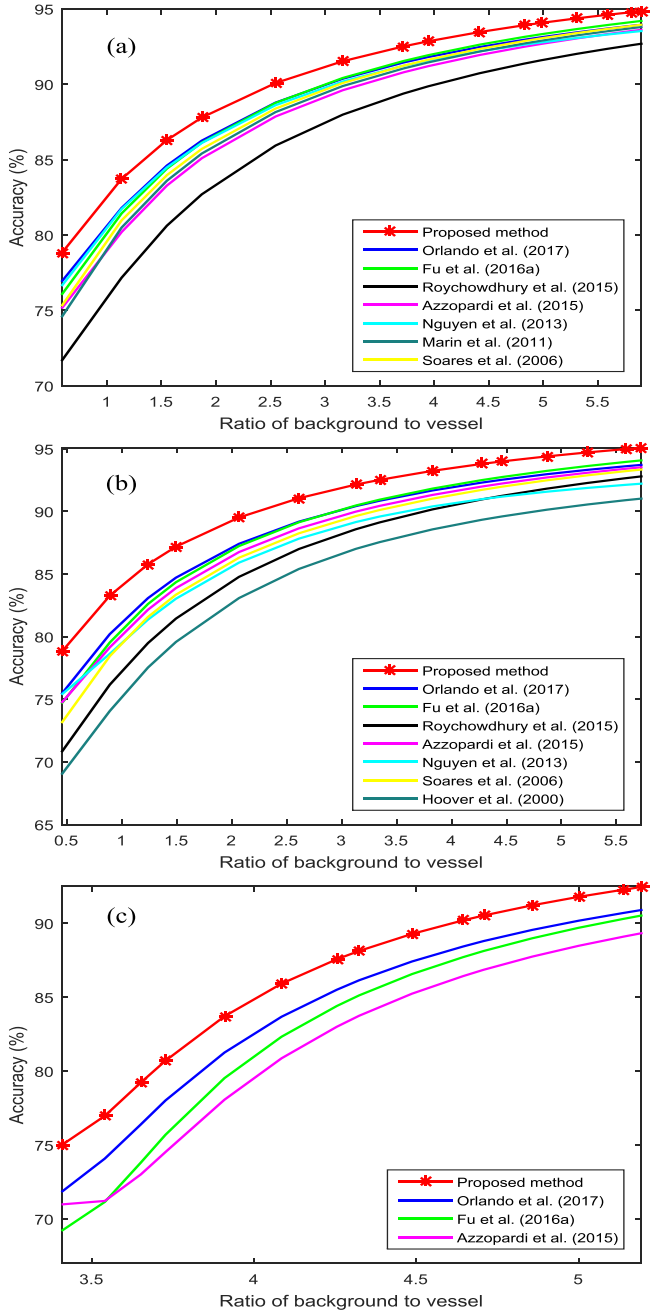

Fig. 6. Local ACC of different methods with the different ratio of the number of pixels of background to that of vessel. (a) DRIVE database. (b) STARE database. (c) CHASE_DB1 database.

3.4.3. Peripapillary vessel analysis

Vessel in and around the optic disk are referred to be the peripapillary vessel, whose structure changes can lead to many retinal abnormalities like glaucoma, central retinal vein occlusion. Existing methods often perform less well due to the effect of packed nerve heads [24]. We carry out the proposed framework on those peripapillary vessel and compare our performance with other state-of-the-art methods. A mask for peripapillary region is delineated manually around the optic disk in each fundus image on DRIVE, STARE and CHASE_DB1 databases respectively. For STARE database, we only perform peripapillary vessel analysis on the first 19 images because the last image from the STARE database does not contain the peripapillary region [5]. Table 4 shows the comparison result of peripapillary vessel detection. Values of the state-of-art methods are computed from the images provided by the corresponding literatures. Compared to those well-known vessel segmentation algorithms, our proposed framework exhibits the best performance on the detection of peripapillary vessel consistently on three databases.

Table 4
Peripapillary vessel segmentation performance on DRIVE, STARE and CHASE_DB1 databases(%).

Database	Method	ACC	ACC_l	F1	MCC
DRIVE	Soares et al. [16]	87.91	79.54	81.21	72.69
	Marin et al. [19]	88.94	80.65	81.76	75.30
	Nguyen et al. [4]	88.05	82.55	82.53	73.45
	Roychowdhury et al. [5]	89.76	82.13	83.15	77.25
	Azzopardi et al. [51]	90.19	83.39	85.55	78.14
	Fu et al. [34]*	90.24	83.28	86.42	79.04
	Orlando et al. [18]	89.30	82.73	85.17	77.08
	Proposed method	**91.80**	**86.66**	**87.88**	**81.70**
STARE	Hoover et al. [49]	83.40	72.21	65.78	54.86
	Soares et al. [16]	83.24	76.71	67.54	56.34
	Nguyen et al. [4]	85.15	79.14	72.27	62.50
	Azzopardi et al. [51]	88.18	78.70	73.72	66.83
	Fu et al. [34]*	88.69	79.52	76.94	69.46
	Orlando et al. [18]	84.74	80.61	71.46	61.40
	Proposed method	**89.71**	**81.31**	**77.71**	**84.25**
CHASE_DB1	Azzopardi et al. [51]	89.53	79.90	81.65	74.35
	Fu et al. [34]*	86.66	79.90	81.65	74.35
	Orlando et al. [18]	88.69	79.62	80.79	72.83
	Proposed method	**91.33**	**83.36**	**85.10**	**79.13**

* Result produced by deep learning based method.

Table 5
Performance comparison on thin vessel and low-contrast vessel in STARE database (%).

Method	Thin vessel			Low-contrast vessel		
	ACC	F1	MCC	ACC	F1	MCC
Hoover et al. [49]	72.64	51.50	32.83	94.13	53.73	50.66
Soares et al. [16]	81.22	60.05	48.40	96.22	61.95	61.72
Nguyen et al. [4]	76.01	60.72	45.07	96.03	68.67	66.63
Azzopardi et al. [51]	76.71	58.79	42.99	96.10	65.96	64.00
Fu et al. [34]*	79.30	55.19	42.53	96.26	61.33	61.69
Orlando et al. [18]	80.64	59.43	47.14	96.49	64.96	64.78
Proposed method	**83.38**	**64.89**	**54.57**	**97.09**	**72.29**	**71.73**

* Result produced by deep learning based method.

3.4.4. Thin vessel and low-contrast vessel analysis

We investigate the segmentation effectiveness of the proposed method on two challenging vessels, i.e. thin vessel and low-contrast vessel. Vessels with width less than 3 pixels are delineated as thin vessel. Background regions around thin vessel within 2 pixels from the vessel edges are taken to assess the proposed method on thin vessel segmentation. Table 5 shows the performance comparison results on thin vessel segmentation, where the proposed method outperforms other methods consistently on three measurements, i.e. achieving performance gains of 2.2% for ACC, 4.2% for F1 and 6.2% for MCC from the best performances of the compared existing approaches. To evaluate the segmentation performance on low-contrast retinal vessel, we search a set of subregions containing low contrast vessel throughout all retinal images, and report their segmentation performance in Table 5. The results show that our proposed method produces the best segmentation performance for low-contrast vessel consistently on three measurements. From the detailed quantitative experimental analyses in Table 5, we exemplify the effectiveness of the proposed method on the detection of the challenging thin vessel and low-contrast vessel.

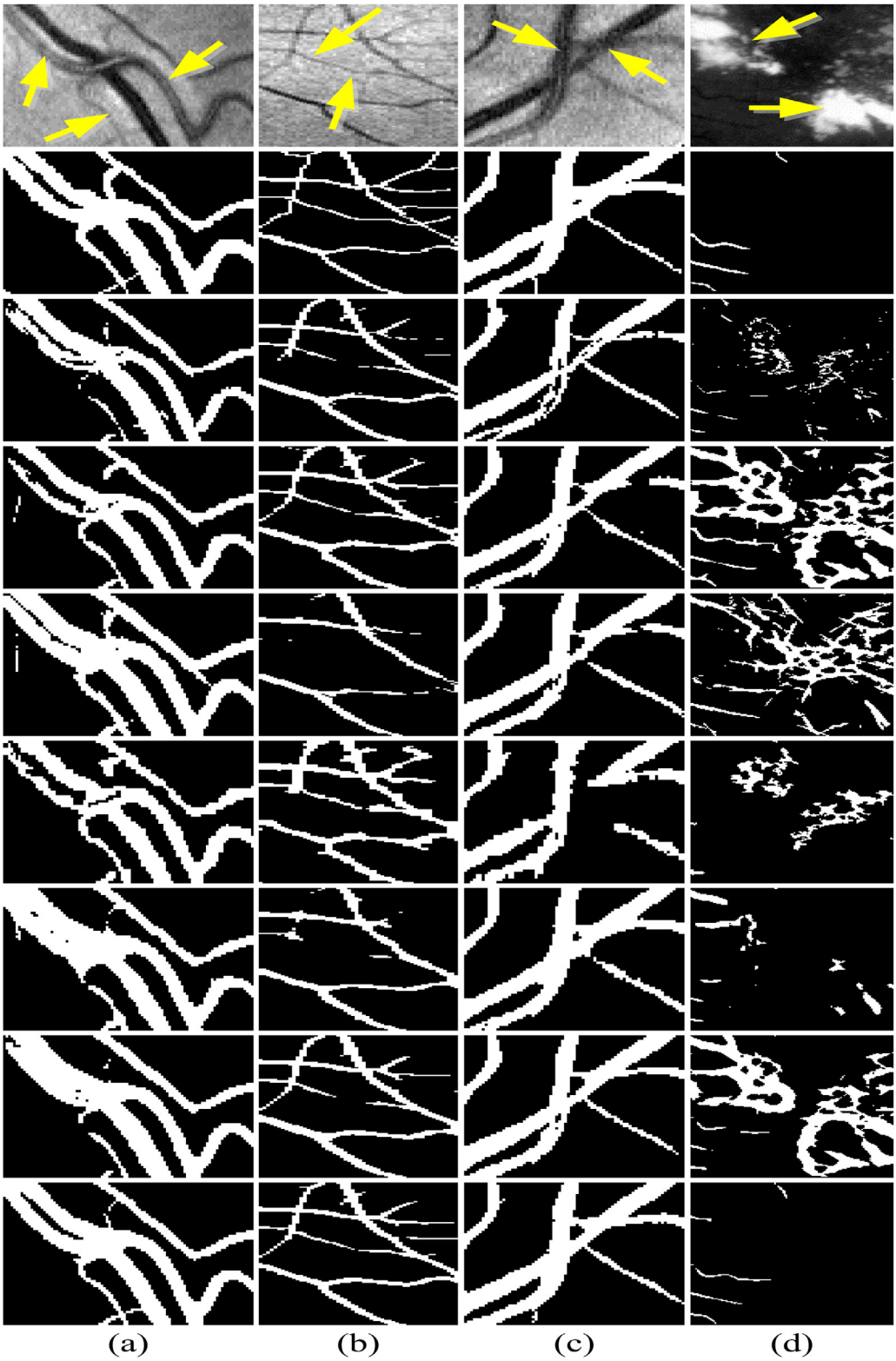

Fig. 7. Comparisons with the state-of-the art methods under some specific challenging and difficult conditions of retinal image. (a) Parallel vessels. (b) Vessels with low contrast. (c) Crossing vessels. (d) Lesions. The first row to the last row: subregions of retinal images, ground truths, segmented results by [4,5,16,18,34,51], and the proposed method, respectively.

3.4.5. Pathological retinal image analysis

To evaluate the performance of the proposed method on pathological retinal image, we conduct experiment on ten abnormal images in STARE database. Those abnormal images have lesions such as hemorrhages and exudates that are difficult for segmentation system to correctly detect retinal vessel. Table 6 shows our comparison results with other methods, where we achieve the significantly improvement on pathological retinal image segmentation. Especially for MCC, the proposed method yields an improvement of 3.6% that indicates the proposed method can effectively distin-

Table 6
Performance comparison on pathological retinal image in STARE database (%).

Method	ACC	ACC_l	F1	MCC
Hoover et al. [49]	92.12	77.06	61.01	56.91
Soares et al. [16]	94.18	79.64	68.36	65.15
Nguyen et al. [4]	91.93	79.92	64.16	61.05
Azzopardi et al. [51]	94.76	80.89	72.17	69.29
Orlando et al. [18]	93.93	80.59	68.35	65.05
Fu et al. [34]*	95.70	80.52	75.38	73.21
Proposed method	**96.29**	**83.68**	**78.71**	**76.85**

* Result produced by deep learning based method.

Table 7
Segmentation performance on HRF database (%).

Method	ACC	ACC_l	F1	MCC
Orlando et al. [18]	94.78	73.28	71.58	68.97
Yan et al. [35]*	94.37	N.A	N.A	N.A
Singel SVM	95.30	73.07	72.11	70.85
Proposed method	**95.73**	**74.98**	**74.74**	**72.88**

* Result produced by deep learning based method.

guish vessel from complex background. High segmentation performance on pathological retinal image also shows the capacity of the proposed method on clinical diagnosis of retinal vessel disease.

3.4.6. High-resolution retinal image analysis

We also assess the proposed method on high-resolution fundus database. Table 7 shows the segmentation performance, where the proposed architecture enhances the performance of naive SVM classifier by 0.2% of ACC, 1.9% of ACC_l, 2.6% of F1 and 2.0% of MCC. It indicates the validity of the proposed method on high-resolution retinal image segmentation. Furthermore, experimental results compared to other state-of-art methods show the superiority of the proposed method on high-resolution retinal image segmentation. This effectiveness and robustness of the proposed method to the retinal image resolution is beneficial for extending it to other retinal images captured by different fundus cameras.

4. Conclusion

In this paper, we have proposed a new divide-and-conquer funnel-structured classification framework for retinal vessel segmentation. By dividing the retinal vessel pixels into well constrained subsets where samples with similar geometrical property are grouped together, the sample variation in each subset is largely reduced. This decomposes a complex classification problem into a number of relatively simpler ones. Training a set of homogeneous classifiers in parallel not only reduces the computational cost like time and storage, but also simplifies the classification complexity because samples at the same subset have smaller variation. With the proposed funnel-structured vessel segmentation framework, we alleviate the problem caused by the imperfect data partition in the dividing phase. This further enhances the complexity and discriminative capability of the proposed whole decision model. Experiments on three diverse databases show the superiority of the proposed framework for vessel segmentation, achieving the best performance consistently in terms of four different evaluation metrics on all three databases. Even for complex vessel structures, the proposed framework also displays very good detection ability. High accuracy for peripapillary blood vessel extraction makes the proposed framework a suitable tool for the computer-aided screening for early diseases detection like glaucoma, and vein occlusion. The demonstrated flexibility, robustness and effectiveness suggests a good potential of the proposed framework in real clinic application of the automated retinal image analysis.

Conflict of interest

None.

References

[1] M.E. Martinez-Perez, A.D. Hughes, S.A. Thom, A.A. Bharath, K.H. Parker, Segmentation of blood vessels from red-free and fluorescein retinal images, Med. Image Anal. 11 (1) (2007) 47–61.
[2] G. Kovács, A. Hajdu, A self-calibrating approach for the segmentation of retinal vessels by template matching and contour reconstruction, Med. Image Anal. 29 (2016) 24–46.
[3] E. Kerrien, A. Yureidini, J. Dequidt, C. Duriez, R. Anxionnat, S. Cotin, Blood vessel modeling for interactive simulation of interventional neuroradiology procedures, Med. Image Anal. 35 (2017) 685–698.
[4] U.T. Nguyen, A. Bhuiyan, L.A. Park, K. Ramamohanarao, An effective retinal blood vessel segmentation method using multi-scale line detection, Pattern Recognit. 46 (3) (2013) 703–715.
[5] S. Roychowdhury, D.D. Koozekanani, K.K. Parhi, Iterative vessel segmentation of fundus images, IEEE Trans. Biomed. Eng. 62 (7) (2015) 1738–1749.
[6] E. Bekkers, R. Duits, T. Berendschot, B. ter Haar Romeny, A multi-orientation analysis approach to retinal vessel tracking, J. Math. Imaging Vis. 49 (3) (2014) 583–610.
[7] Y. Yin, M. Adel, S. Bourennane, Retinal vessel segmentation using a probabilistic tracking method, Pattern Recognit. 45 (4) (2012) 1235–1244.
[8] A.M. Mendonca, A. Campilho, Segmentation of retinal blood vessels by combining the detection of centerlines and morphological reconstruction, IEEE Trans. Med. Imaging 25 (9) (2006) 1200–1213.
[9] M.S. Miri, A. Mahloojifar, Retinal image analysis using curvelet transform and multistructure elements morphology by reconstruction, IEEE Trans. Biomed. Eng. 58 (5) (2011) 1183–1192.
[10] Y.Q. Zhao, X.H. Wang, X.F. Wang, F.Y. Shih, Retinal vessels segmentation based on level set and region growing, Pattern Recognit. 47 (7) (2014) 2437–2446.
[11] Y.T. Zhao, L. Rada, K. Chen, S.P. Harding, Y. Zheng, Automated vessel segmentation using infinite perimeter active contour model with hybrid region information with application to retinal images, IEEE Trans. Med. Imaging 34 (9) (2015) 1797–1807.
[12] A. Gooya, H. Liao, K. Matsumiya, K. Masamune, Y. Masutani, T. Dohi, A variational method for geometric regularization of vascular segmentation in medical images, IEEE Trans. Image Process. 17 (8) (2008) 1295–1312.
[13] X. Xu, M. Niemeijer, Q. Song, M. Sonka, M.K. Garvin, J.M. Reinhardt, M.D. Abràmoff, Vessel boundary delineation on fundus images using graph-based approach, IEEE Trans. Med. Imaging 30 (6) (2011) 1184–1191.
[14] J. De, L. Cheng, X. Zhang, F. Lin, H. Li, K.H. Ong, W. Yu, Y. Yu, S. Ahmed, A graph-theoretical approach for tracing filamentary structures in neuronal and retinal images, IEEE Trans. Med. Imaging 35 (1) (2016) 257–272.
[15] J. Staal, M.D. Abràmoff, M. Niemeijer, M. Viergever, B.V. Ginneken, Ridge-based vessel segmentation in color images of the retina, IEEE Trans. Med. Imaging 23 (4) (2004) 501–509.
[16] J.V. Soares, J.J. Leandro, R.M. Cesar, H.F. Jelinek, M.J. Cree, Retinal vessel segmentation using the 2-d Gabor wavelet and supervised classification, IEEE Trans. Med. Imaging 25 (9) (2006) 1214–1222.
[17] X. You, Q. Peng, Y. Yuan, Y.M. Cheung, J. Lei, Segmentation of retinal blood vessels using the radial projection and semi-supervised approach, Pattern Recognit. 44 (10) (2011) 2314–2324.
[18] J. Orlando, E. Prokofyeva, M. Blaschko, A discriminatively trained fully connected conditional random field model for blood vessel segmentation in fundus images, IEEE Trans. Biomed. Eng. 64 (1) (2017) 16–27.
[19] D. Marín, A. Aquino, M.E. Gegúndez-Arias, J.M. Bravo, A new supervised method for blood vessel segmentation in retinal images by using gray-level and moment invariants-based features, IEEE Trans. Med. Imaging 30 (1) (2011) 146–158.
[20] R. Vega, G. Sanchez-Ante, L.E. Falcon-Morales, H. Sossa, E. Guevara, Retinal vessel extraction using lattice neural networks with dendritic processing, Comput. Biol. Med. 58 (2015) 20–30.
[21] S. Wang, Y. Yin, G. Cao, B. Wei, Y. Zheng, G. Yang, Hierarchical retinal blood vessel segmentation based on feature and ensemble learning, Neurocomputing 149 (2015) 708–717.
[22] J. Zhang, Y. Chen, E. Bekkers, M. Wang, B. Dashtbozorg, B. ter Haar Romeny, Retinal vessel delineation using a brain-inspired wavelet transform and random forest, Pattern Recognit. 69 (2017) 107–123.
[23] M.M. Fraz, P. Remagnino, A. Hoppe, B. Uyyanonvara, A.R. Rudnicka, C.G. Owen, S. Barman, An ensemble classification-based approach applied to retinal blood vessel segmentation, IEEE Trans. Biomed. Eng. 59 (9) (2012) 2538–2548.
[24] L. Gu, X. Zhang, H. Zhang, H. Li, L. Cheng, Segment 2d and 3d filaments by learning structured and contextual features, IEEE Trans. Med. Imaging 36 (2) (2017) 596–606.
[25] B. Barkana, I. Saricicek, B. Yildirim, Performance analysis of descriptive statistical features in retinal vessel segmentation via fuzzy logic, ANN, SVM, and classifier fusion, Knowl Based Syst 118 (2017) 165–176.
[26] X. Wang, X. Jiang, J. Ren, Blood vessel segmentation from fundus image by a cascade classification framework, Pattern Recognit. 88 (2019) 331–341.
[27] H. Ding, X. Jiang, B. Shuai, A. Liu, G. Wang, Context contrasted feature and gated multi-scale aggregation for scene segmentation, in: Proc. IEEE Conf. Comput. Vis. Pattern Recognit., 2018, pp. 2393–2402.

[28] B. Shuai, H. Ding, T. Liu, G. Wang, X. Jiang, Toward achieving robust low-level and high-level scene parsing, IEEE Trans. Image Process. 28 (3) (2019) 1378–1390.
[29] K. He, X. Zhang, S. Ren, J. Sun, Deep residual learning for image recognition, in: Proceedings of the IEEE Conference on Computer Vision and Pattern Recognition, 2016, pp. 770–778.
[30] Q. Li, B. Feng, L. Xie, P. Liang, H. Zhang, T. Wang, A cross-modality learning approach for vessel segmentation in retinal images, IEEE Trans. Med. Imaging 35 (1) (2016) 109–118.
[31] P. Liskowski, K. Krawiec, Segmenting retinal blood vessels with deep neural networks, IEEE Trans. Med. Imaging 35 (11) (2016) 2369–2380.
[32] H. Fu, Y. Xu, D. Wong, J. Liu, Retinal vessel segmentation via deep learning network and fully-connected conditional random fields, in: Proc. 9th Int. Symp. Biomed. Imaging, 2016, pp. 698–701.
[33] K. Maninis, P. Jordi, A. Pablo, V. Luc, Deep retinal image understanding, in: Proc. 19th Med. Image Comput. Comput. Assist. Interv., 2016, pp. 140–148.
[34] H. Fu, Y. Xu, S. Lin, D. Wong, J. Liu, DeepVessel: retinal vessel segmentation via deep learning and conditional random field, in: Proc. 19th Med. Image Comput. Comput. Assist. Interv., 2016, pp. 132–139.
[35] Z. Yan, X. Yang, K. Cheng, Joint segment-level and pixel-wise losses for deep learning based retinal vessel segmentation, IEEE Trans. Biomed. Eng. 65 (9) (2018) 1912–1923.
[36] A. Oliveira, S. Pereira, C. Silva, Retinal vessel segmentation based on fully convolutional neural networks, Expert Syst. Appl. 112 (2018) 229–242.
[37] K. Hu, Z. Zhang, X. Niu, Y. Zhang, C. Cao, F. Xiao, X. Gao, Retinal vessel segmentation of color fundus images using multiscale convolutional neural network with an improved cross-entropy loss function, Neurocomputing 309 (2018) 179–191.
[38] Z. Yan, X. Yang, K. Cheng, A three-stage deep learning model for accurate retinal vessel segmentation, IEEE J. Biomed. Health Inf. doi:10.1109/JBHI.2018.2872813.
[39] L. Yu, Z. Qin, T. Zhuang, Y. Ding, Z. Qin, K. Choo, A framework for hierarchical division of retinal vascular networks, Neurocomputing. doi:10.1016/j.neucom.2018.11.113.
[40] S. Feng, Z. Zhuo, D. Pan, Q. Tian, CcNet: a cross-connected convolutional network for segmenting retinal vessels using multi-scale features, Neurocomputing. doi:10.1016/j.neucom.2018.10.098.
[41] S. Chaudhuri, S. Chatterjee, N. Katz, M. Nelson, M. Goldbaum, Detection of blood vessels in retinal images using two-dimensional matched filters, IEEE Trans. Med. Imaging 8 (3) (1989) 263–269.
[42] X. Wang, X. Jiang, Nonlinear retinal image enhancement for vessel detection, in: Proc. 9th Int. Conf. Digital Image Process., vol. 10420, 2017, p. 104202M.
[43] X. Wang, X. Jiang, Enhancing retinal vessel segmentation by color fusion, in: Proc. 42nd Int. Conf. Acoust. Speech Signal Process., 2017, pp. 891–895.
[44] X. Jiang, Image detail-preserving filter for impulsive noise attenuation, IEE Proc.-Vis. Image Signal Process. 150 (3) (2003) 179–185.
[45] A.F. Frangi, W.J. Niessen, K.L. Vincken, M.A. Viergever, Multiscale vessel enhancement filtering, in: Proc. 1st Med. Image Comput. Comput. Assist. Interv., 1998, pp. 130–137.
[46] L. Tang, M. Niemeijer, J.M. Reinhardt, M.K. Garvin, M.D. Abràmoff, Splat feature classification with application to retinal hemorrhage detection in fundus images, IEEE Trans. Med. Imaging 32 (2) (2013) 364–375.
[47] X. Jiang, Asymmetric principal component and discriminant analyses for pattern classification, IEEE Trans. Pattern Anal. Mach. Intell. 31 (5) (2009) 931–937.
[48] X. Wang, X. Jiang, Post-processing for retinal vessel detection, in: Proc. 10th Int. Conf. Digital Image Process., vol. 10806, 2018, p. 1080656.
[49] A. Hoover, V. Kouznetsova, M. Goldbaum, Locating blood vessels in retinal images by piecewise threshold probing of a matched filter response, IEEE Trans. Med. Imaging 19 (3) (2000) 203–210.
[50] J. Odstrcilik, R. Kolar, A. Budai, J. Hornegger, J. Jan, J. Gazarek, T. Kubena, P. Cernosek, O. Svoboda, E. Angelopoulou, Retinal vessel segmentation by improved matched filtering: evaluation on a new high-resolution fundus image database, IET Image Process. 7 (4) (2013) 373–383.
[51] G. Azzopardi, N. Strisciuglio, M. Vento, N. Petkov, Trainable COSFIRE filters for vessel delineation with application to retinal images, Med. Image Anal. 19 (1) (2015) 46–57.